

Evaluation on out-of-plane shear stiffness and ultimate capacity of perfobond connector

Liu, Yangqing; Wang, Sihao; Xin, Haohui; Liu, Yuqing

DOI

[10.1016/j.jcsr.2019.105850](https://doi.org/10.1016/j.jcsr.2019.105850)

Publication date

2020

Document Version

Final published version

Published in

Journal of Constructional Steel Research

Citation (APA)

Liu, Y., Wang, S., Xin, H., & Liu, Y. (2020). Evaluation on out-of-plane shear stiffness and ultimate capacity of perfobond connector. *Journal of Constructional Steel Research*, 167, Article 105850. <https://doi.org/10.1016/j.jcsr.2019.105850>

Important note

To cite this publication, please use the final published version (if applicable). Please check the document version above.

Copyright

Other than for strictly personal use, it is not permitted to download, forward or distribute the text or part of it, without the consent of the author(s) and/or copyright holder(s), unless the work is under an open content license such as Creative Commons.

Takedown policy

Please contact us and provide details if you believe this document breaches copyrights. We will remove access to the work immediately and investigate your claim.



Evaluation on out-of-plane shear stiffness and ultimate capacity of perfobond connector



Yangqing Liu^a, Sihao Wang^a, Haohui Xin^{a,b}, Yuqing Liu^{a,*}

^a College of Civil Engineering, Tongji University, Shanghai, China

^b Faculty of Civil Engineering and Geosciences, Delft University of Technology, Netherlands

ARTICLE INFO

Article history:

Received 24 August 2019

Received in revised form

12 October 2019

Accepted 2 November 2019

Available online 27 November 2019

Keywords:

Composite structures

Perfobond connector

Push-out test

Finite element analysis

Lateral shear stiffness

Lateral shear capacity

ABSTRACT

Perfobond shear connectors (PBLs) are increasingly applied in steel-concrete composite structures. The out-of-plane (lateral) shear behavior of PBLs is still unknown to researchers and designers, although the connectors undertake considerable out-of-plane shear forces in some applications. Thus, push-out tests with three specimens were first conducted to investigate the lateral shear performance of PBLs and further used to validate the corresponding numerical models. The test results show that perforated rebars and concrete dowels are irrelevant to the lateral shear capacity, while they can reduce the separations and improve the ductility. Secondly, parametric FEA (finite element analysis) models for the push-out tests were built and validated based on the test results. The plastic strains in concrete mainly develop at the regions close to the fillet welds. Further, 144 extended FEA models with varying height, length, and thickness of perfobond plates and concrete compressive strength were conducted to reveal the lateral shear mechanism of PBLs. By enlarging the plate height, the lateral shear capacity slightly increases, while the shear stiffness remains as constant. The shear capacity and stiffness increase with the plate length and thickness, as well as the concrete compressive strength. Finally, based on the existing shear capacity equations for channel and angle connectors, and the theory of elastic foundation beams, the expressions for the lateral shear capacity and stiffness of PBLs were put forward. The proposed equations agree with the results of the parametric study.

© 2019 Elsevier Ltd. All rights reserved.

1. Introduction

Perfobond shear connectors (PBLs) are increasingly applied in composite structures due to their high shear capacity and excellent fatigue performance [1,2], such as the PBLs used in the composite truss joints [1], the hybrid girder joints [3–5], the hybrid pylon joints [6,7], the anchorage joints between suspenders and girders [2], and the lower slab of composite girders with corrugated webs [8]. Fig. 1 shows an application of PBLs in corrugated web composite girders, which usually use large web spacing and overhang length so that the transverse moments and shears are considerable. PBLs are employed on the top and bottom flanges to connect the concrete slabs with the flanges. Fig. 1(b) presents the load path in the transverse direction, where the PBLs on the top flanges are under out-of-plane shear forces induced from the transverse moment. Also, since the PBLs on the bottom flanges are placed perpendicular to the longitudinal direction of girders, they should have sufficient

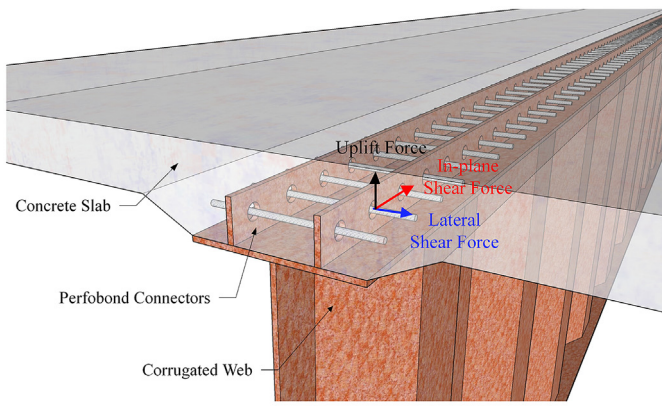
lateral shear capacity and stiffness.

In the past two decades, researchers investigated the longitudinal shear behavior of PBLs by push-out tests and finite element analyses (FEA) [9–14]. The results showed that the shear behavior of PBLs is mainly relevant to the diameter of holes and perforated rebars, as well as the strength of concrete and perforated rebars. The number of holes, the bond between steel and concrete, bearing forces at plate ends, and transverse reinforcements also affect the shear behavior. Shear capacity equations with different forms were put forward by regression and neural network analyses [15]. Recently, the shear performance of PBLs under different loading and made of varying material were investigated, including under cyclic fatigue loading [1], exposed to the high temperature [16], made of the lightweight concrete [17], made of the fiber-reinforced concrete [18] and made of the GFRP perfobond plates [19]. Also, some novel geometries and details were proposed to improve the shear distribution and constructional convenience of PBL groups, including the Y-type PBLs [20], notched PBLs [21], rubber-ring PBLs [22].

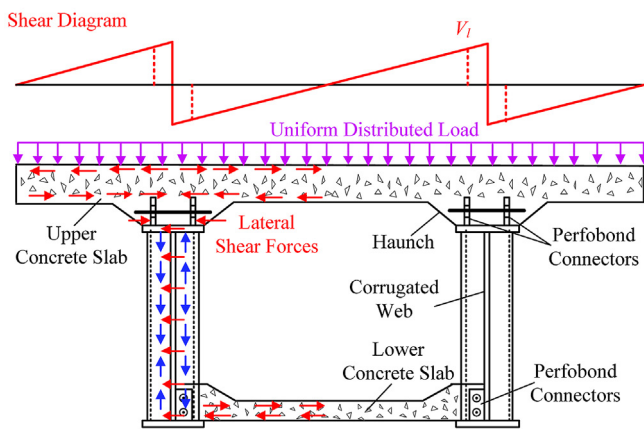
However, the evaluation of the out-of-plane shear capacity and stiffness of PBLs are limited as far as the authors' knowledge. The

* Corresponding author.

E-mail address: yql@tongji.edu.cn (Y. Liu).



(a) Force state



(b) Load path*

Fig. 1. Applications of perfbond connectors. * The amplitude and direction of transverse shears in webs are dependent to the width of slabs, the layout and stiffness of PBLs.

lateral shear behavior dominates the structural behavior of the connection interfaces or joints under the transverse moment. Besides, for the massive and complex composite structures, it's unrealistic to establish the full-solid FEA models considering all the details of PBLs to evaluate the combined performance of connections. An alternative option is to model the connectors via elastic or inelastic spring elements, which can significantly reduce computational time and cost. The force-slip relationships along three directions need to be known by researchers and designers. Zheng et al. [23] proposed an expression for the longitudinal force-slip relationships of PBLs based on push-out tests. However, the factors that affect the lateral shear stiffness are still unclear. It is important to investigate the lateral shear performance of PBLs to make sure a safe design.

In this paper, three push-out tests taking the provisions of perforated rebars and concrete dowels into account were first carried out to investigate the out-of-plane shear behavior of PBLs. The failure modes, shear force-slip curves, and shear force-separation curves were obtained and discussed. Secondly, 3D parametric FE models for the push-out tests were built and validated by the test results. The bending stress on perfbond plates and the distribution of plastic strains in concrete blocks were analyzed. Further, 144 extended FE models with varying height, length, and thickness of perfbond plates and concrete grades were

conducted to reveal the lateral shear mechanism of PBLs. Finally, the expressions for the lateral shear capacity and stiffness of PBLs were put forward based on the existing shear capacity equations for channel and angle connectors, and the theory of elastic foundation beams. The proposed equations agree with the numerical results.

2. Push-out tests

2.1. Test specimens

In this section, the push-out tests for the lateral shear behavior of PBLs are described, including the specimen configuration, test setup and instrumentation, material properties, and test results.

Table 1 presents the dimensions of the specimens, where d and d_s are the diameters of holes and perforated rebars; A_c is the area of concrete dowels; l , h , and t are the length, height, and thickness of perfbond plates, respectively. Specimen LSP-1 represents the ordinary PBL loaded by lateral shear forces. In Specimen LSP-2, the perforated rebar was removed to investigate the effects of perforated rebars on the lateral shear behavior. Compared with LSP-2, the holes of perfbond plates in Specimen LSP-3 were filled by foams before concrete casting, so that the contributions of concrete dowels could be drawn.

Fig. 2 shows the specimen configuration. The built-up steel beam consisted of two 400 mm × 500 mm × 30 mm flanges and a 200 mm × 460 mm × 30 mm web. The clearance under the steel beam was 50 mm to guarantee that the specimens had sufficient space to slip. On both sides of the specimens, a perfbond plate with the size of 150 mm × 250 mm × 20 mm was horizontally welded on the flanges of steel beams. The concrete blocks had a dimension of 500 mm × 500 mm × 500 mm to consider the haunch above top flanges in composite bridge applications. Distributed reinforcements with a diameter of 16 mm were also located inside the concrete blocks to prevent unexpected cracking of concrete. In total, the amount of steel and concrete used for one specimen was 0.14 metric ton and 0.125 m³, respectively.

2.2. Test setup and instrumentation

Fig. 3 shows the test setup and instrumentation. The specimens were loaded by the servo-hydraulic machine. In order to make the applied loads and the reaction forces uniform, the concrete blocks were placed on a sand cushion. A rigid distributed beam was set between the loading machine and the specimens. To obtain the slips and separations between the perfbond plates and the concrete blocks, four vertical and horizontal LVDTs with 1/1000 mm precision were mounted between the flanges of steel beams and concrete blocks. Four small angles were stuck on the side surfaces of concrete blocks at the same height as perfbond plates to locate the vertical LVDTs. The horizontal LVDTs directly contacted with the concrete blocks.

The test loading consisted of the force-controlled cyclic preloading stage and the displacement-controlled monotonic loading stage. According to Eurocode 4 [24], the loads ranged from 5% to 40% of the estimated ultimate capacity in the preloading stage. The loading speed was controlled as 3 kN/s. Subsequently, the formal monotonic loading with the loading speed of 0.3 mm/min was conducted. The total time from the beginning of loading to the failure of specimens was more than 30 min.

2.3. Material properties

During the casting, three groups of twelve concrete samples were fabricated to evaluate the concrete properties, including 150 × 150 × 150 mm cubes, 150 × 150 × 300 mm cylinders and prisms. Concrete with the grade of C50 [25], which supposed the

cube compressive strength should be higher than 50 MPa was used for the specimens. Table 2 shows the concrete properties from material tests, where f_{cu} , f_c , and f_c' are the cube, cylinder, and prism compressive strength, respectively; f_t and E_c are the splitting tensile strength and elastic modulus. The nominal yield strength of the steel plates and rebars used for the specimens are 345 MPa and 400 MPa. Also, tensile tests on three groups of rebars with varying diameters and plate coupons with different thicknesses were carried out to obtain the steel properties. There were three samples in each group. Table 3 shows the average yield strength, tensile strength, and elastic modulus of each group.

2.4. Test results

Table 4 summarizes the test results, where V_l and k_l are the lateral shear capacity and stiffness for single perfobond connector. The shear stiffness is defined as the secant slope when the slip equals 0.2 mm [23]. s_l and u_l are the peak slip and separation corresponding to the shear capacity. The difference in the shear capacities among the specimens is within 3%. It indicates that perforated rebars and concrete dowels are irrelevant to the lateral shear capacity of PBLs. Compared with LSP-1, the shear stiffness of LSP-2 and LSP-3 reduce 7.7% and 13.6%, while the peak separations of LSP-2 and LSP-3 increase 17% and 41%. Since the parameters are the perforated rebars and concrete dowels, which can decrease the separations between steel beams and concrete, the reduction in the lateral shear stiffness results from the increasing separations.

Fig. 4 (a) and (b) show the failure modes of concrete blocks and perfobond plates. The majorities of cracks were vertically distributed near the positions of perfobond plates and the regions under the plates. As the slip increased, the widths of the cracks under the plates significantly grew. Even part of the concrete fell off, indicating that the concrete in the region close to the steel beam undertook most of the applied load. The reaction forces concentrated at the corner of the bottom surface of concrete blocks. Fig. 4(b) illustrates that the perfobond plates of all the specimens had a visible plastic deformation but not fractured. The concrete dowels were sheared off, indicating that the PBLs also undertook large uplift forces as the slips and separations increased. Fig. 5 shows the mechanical model of PBLs under lateral shear forces, where the black and purple arrows are the forces acted on the steel beams and the concrete block, respectively. The applied loads and the supporting forces on the perfobond plates from concrete blocks form additional moments, which lead to the horizontal interaction forces and separations between the steel beams and concrete blocks. The concrete dowels and perforated rebars could help to resist the separation as well as improve the deformation behavior of PBLs under lateral shear loading.

Fig. 6(a) shows the shear force-slip curves of the specimens, which are similar to each other and consist of three stages. The initial stage before 0.2 mm slip displayed in the embedded figure can be roughly considered as a linear part. The plastic stage starts from the end of the linear stage and lasts to the ultimate shear capacity. It is noted that the stiffness reductions of LSP-2 and 3 are more significant than that of LSP-1 in the plastic stage. Although perforated rebars do not contribute to the shear capacity, they can improve the deformation performance. Besides, LSP-1 has higher

remained strength at the decreasing part after the shear capacity, indicating that perforated rebars can also improve the ductility of lateral behavior. The peak slips of all the curves are larger than 3 mm. The reason is that the perfobond plates had yielded before the concrete crushing. The plastic deformation of plates developed, which led to a good lateral ductility of PBLs. Fig. 6(b) displays the shear force-separation curves of the specimens. The same trend is noticeable among the three specimens. The separations are relatively small at the early loading stage. Subsequently, both the slips and separations considerably rise at the plastic stage.

3. FEA and parametric study

3.1. Finite element model

3-D push-out test models for lateral shear behavior of PBLs were established by the commercial finite element software Abaqus/Explicit [26]. Since the test specimens are symmetric in terms of the steel beam central line, only half of the specimens were modeled. Fig. 7 shows finite element models. In the three models, the steel beam, perfobond plate, perforated rebar, and concrete block were simulated by the solid reduced integration element C3D8R. The distributed reinforcements and the ground were built by the truss element T3D2 and the rigid element R3D4 respectively. Compared with the LSP-1 and LSP-2 models, the LSP-3 model included a hollow at the hole to remove the concrete dowel. The boundary conditions of models were consistent with those of the lab tests, including the symmetric boundary condition at the central line of the steel beam and the fixed boundary condition set at the reference point of the ground.

Contact interactions were employed at the interfaces between different components. According to Ref. [14], the frictional coefficient for the interfaces between the concrete blocks and the ground was taken as 0.5. With regards to the contact between steel components and concrete blocks, the fractional coefficient was 0.3. Meanwhile, the uncoupled surface-based cohesive behavior with exponential softening was considered. The bond stiffness, the peak and failure displacement were calibrated as 30 MPa, 0.08 mm and 0.5 mm, and the exponential parameter was taken as 1 [22]. The perforated rebars and the reinforcements were respectively tied and embedded to the concrete blocks [14,22].

3.2. Material model

Since the perfobond plates yielded at the failure of specimens, a trilinear elastic-plastic stress-strain relationship as shown in Fig. 8 was used for the steel plates as well as the perforated rebars and reinforcements [22]. The yield plateau ranged from 1 to 10 times the yield strain ϵ_y , and the ultimate strain ϵ_u was taken as 6% [27]. The concrete property was described by the Concrete Damage Plasticity (CDP) model [26] and the default plastic parameters in the ABAQUS User's Manual. Where the expansion angle was assumed as 37° ; the ratio of biaxial to uniaxial compressive strength was 1.16; the ratio of the second stress invariant on the tensile meridian to that on the compressive meridian was 0.67; the flow potential eccentricity and the viscosity coefficient were 0.1 and 0, respectively.

Fig. 9(a) shows the compressive stress-strain curve used for the concrete blocks. The ascending part of the compressive stress-strain was defined by Eqs. (1) and (2) provided in CEB-FIP MC2010 [27], where ϵ_c and σ_c are the strain and stress at any point on the curve; ϵ_{cp} is the strain corresponding to the peak compressive stress, which is related to f_c . The descending segment is a straight line which ends at the point with 85% of the compressive strength [28]. The value of the corresponding ultimate strain ϵ_{cu} was relevant to f_c , according to CEB-FIP MC2010. With

Table 1
Specimen dimensions.

No.	d (mm)	d_s (mm)	A_c (mm ²)	l (mm)	h (mm)	t (mm)
LSP-1	75	20	4103.7	250	150	20
LSP-2	75	0	4417.9	250	150	20
LSP-3	75	0	0	250	150	20

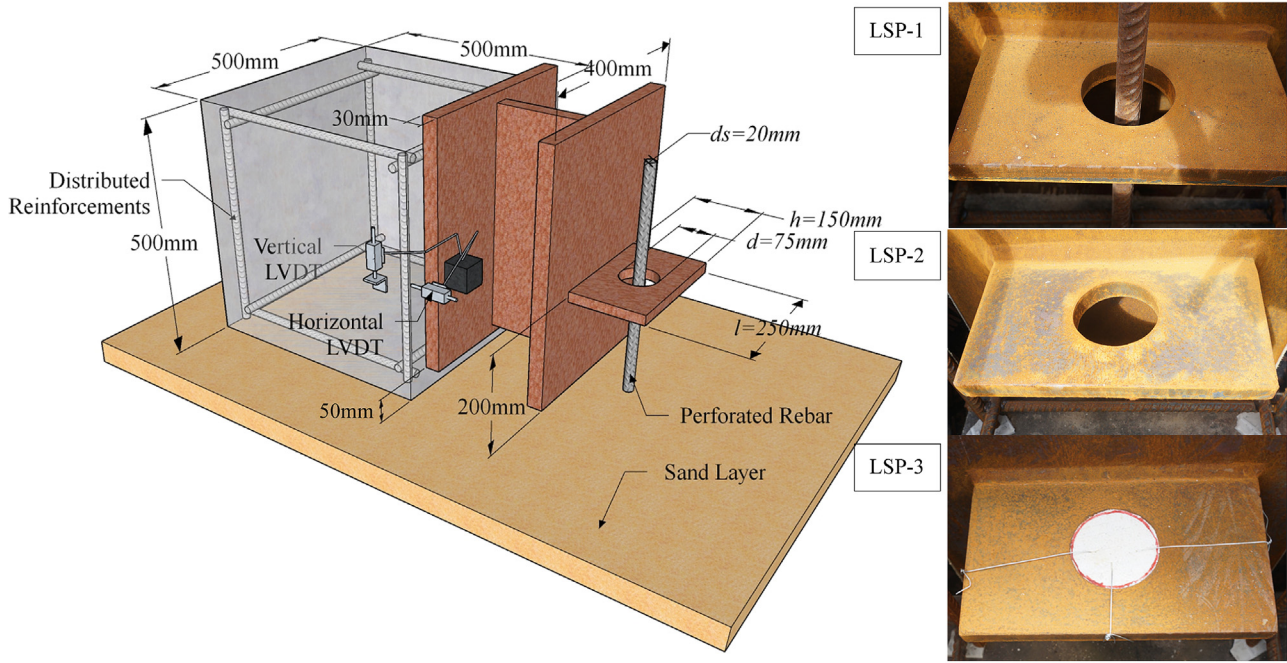


Fig. 2. Specimen configuration.

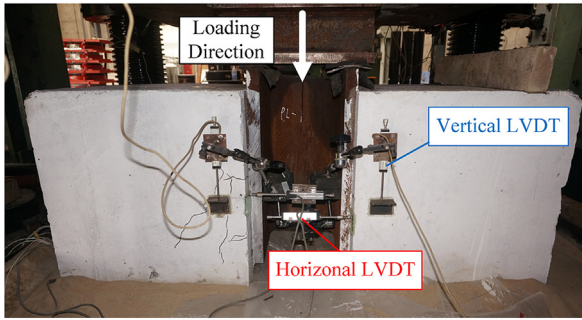


Fig. 3. Test setup and instrumentation.

regards to the tensile behavior, the uncracked concrete was supposed to be linearly elastic. The tensile behavior after cracking was defined by the stress-crack width relationship referred to Hordijk [29], as shown in Fig. 9(b) and Eq. (3).

$$\frac{\sigma_c}{f_c} = \frac{k \cdot \eta - \eta^2}{1 + (k - 2) \cdot \eta} \quad (1)$$

$$k = E_c \cdot \epsilon_{cp} / f_c, \quad \eta = \epsilon_c / \epsilon_{cp} \quad (2)$$

Table 2
Concrete properties.

Group No.	f_{cu} (MPa)	f_c (MPa)	f_c' (MPa)	f_t (MPa)	E_c (GPa)
1	54.46	44.32	45.86	3.87	42.8
2	52.71	43.82	45.16	4.32	44.1
3	54.58	41.63	49.74	4.55	40.9
Mean	53.92	43.26	46.92	4.25	42.6

$$\frac{\sigma_t}{f_t} = \left[1 + \left(c_1 \frac{w}{w_c} \right)^3 \right] \cdot \exp \left(-c_2 \frac{w}{w_c} \right) - \frac{w}{w_c} (1 + c_1^3) \cdot \exp(-c_2) \quad (3)$$

where w and σ_t are the crack width and the tensile stress at any point of the curve; the ultimate crack width $w_c = 5.14 G_F / f_t$ (mm); the fracture energy required to create a unit area of stress-free crack $G_F = 0.073 f_c^{0.18}$ (N/mm); The coefficient c_1 and c_2 were respectively 3 and 6.93.

3.3. Model validation and shear mechanism

3.3.1. Model validation

Fig. 10 compares the experimental shear force-slip and shear force-separation curves with FEA results. Overall, the numerical results agree well with the test results. The FE models are feasible to predict the lateral shear capacity and initial stiffness of PBLs. The simulated curves can reflect the entire shear behavior of the specimens, including the ductile failure process. In the LSP-2 and

Table 3
Steel properties.

	Size	f_y (MPa)	f_u (MPa)	E_s (GPa)
Rebar (HRB400)	$d_s = 16$ mm	526.9	643.8	196.7
	$d_s = 20$ mm	498.6	663.8	199.8
	$d_s = 22$ mm	456.4	618.0	199.5
Plate (Q345)	$t = 16$ mm	356.5	496.5	209.5
	$t = 20$ mm	410.0	545.0	200.0
	$t = 30$ mm	423.0	551.0	200.0

Table 4
Summary of test results.

No.	d (mm)	d_s (mm)	A_c (mm ²)	V_l (kN)	k_l (kN/mm)	s_l (mm)	u_l (mm)
LSP-1	75	20	4103.7	1175.1	2709.6	3.51	0.70
LSP-2	75	0	4417.9	1186.1	2502.2	3.89	0.82
LSP-3	75	0	0	1147.6	2340.2	4.20	0.99

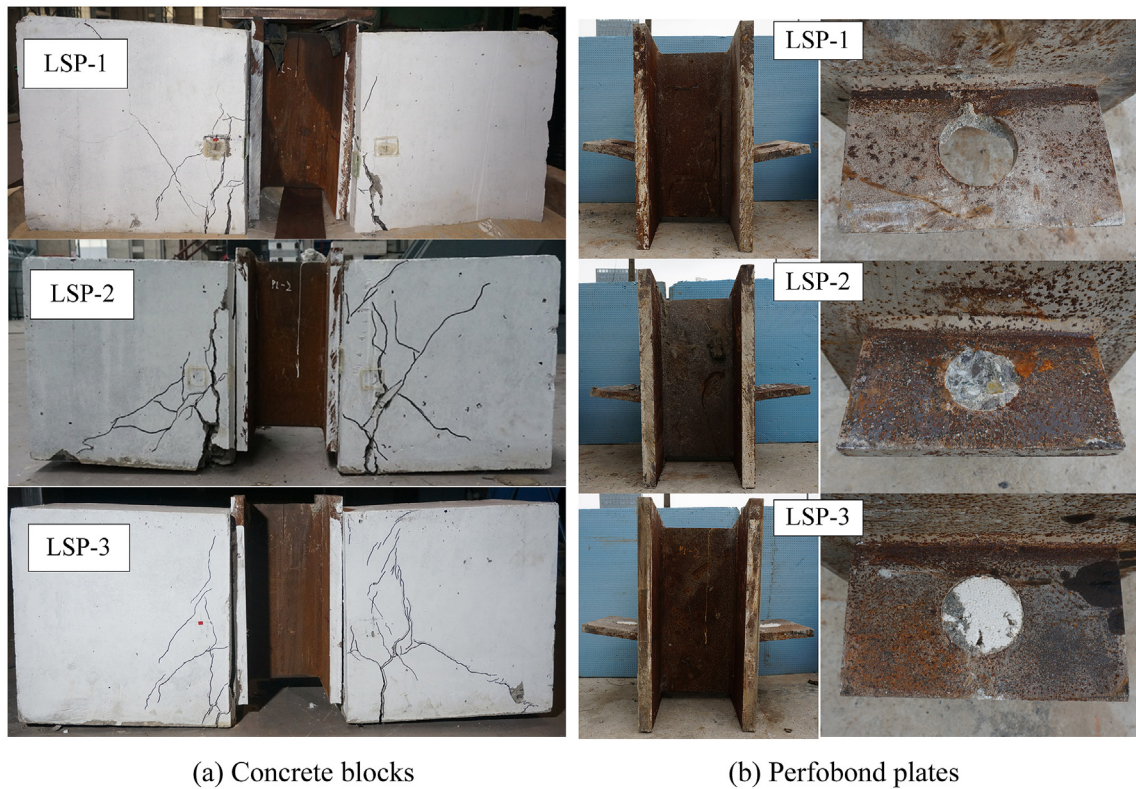


Fig. 4. Failure modes.

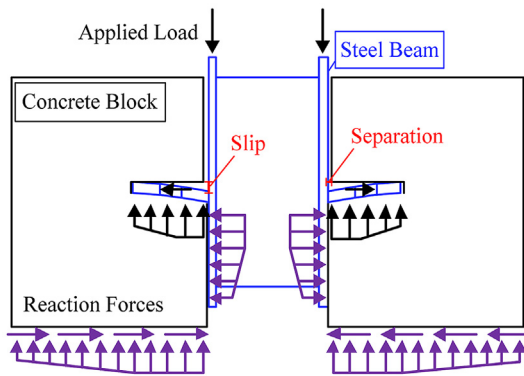


Fig. 5. Mechanical model.

LSP-3 models, the stiffness of the plastic stage is higher than that in the tests. The reason might be that the bond and frictional forces between steel plates and concrete blocks were overestimated in the simulations when the separation increased. Also, the remained shear forces after shear capacities were higher than the test results. This paper focused on the lateral shear capacity and stiffness of PBLs. The ductility and the cohesive behavior should be improved in future works.

3.3.2. Comparison of failure modes

Fig. 11 compares the numerical failure modes with the observed failures in the tests. As illustrated in Fig. 11(a), the perfobond plate yielded close to the fillet welds during the test loading but didn't fracture. Compared with the test specimen, the FE model presents the same deformation shape of the perfobond plate. As for the cracking of concrete blocks, Fig. 11(b) depicts the equivalent plastic strain distribution of the concrete block in the FE model. The

regions with considerable plastic strain are consistent with the positions of cracks in the test. Therefore, the FE results are valid to reveal the failure mode of PBLs under lateral shear loads.

3.3.3. Shear mechanism

Fig. 12(a) shows the bending stress (unit: Pa) on the perfobond plate in the LSP-1 model when the applied load equals the shear capacity. The maximum tensile and compressive stresses which have exceeded the yield strength of plates appear at the regions besides the hole. However, the bending stresses are relatively small at the edge (fillet welds) connected to the steel beam, and the other end of perfobond plates. Paths are defined and shown in Fig. 12(a), where Path-1, 2 and Path-3, 4 are on the top and bottom surface, respectively. Fig. 12(b) plots the bending stresses along the paths. Based on the stress along Path-1 and 2, the major bending regions are 25–75 mm from the fillet welds. However, the positions of fillet welds undertake relatively smaller opposite bending moments, which decrease from the central line of the plate to the two sides along the fillet welds.

Fig. 13 presents the equivalent plastic strains on the concrete blocks under the shear capacity. The plastic strains mainly concentrate at the region close to steel beams with a height of around the plate height. On the contrary, the plastic strains at the end far from the fillet welds are almost 0. The development of plastic strains starts from the corner of perfobond plates and then transfers to the region under the plates by a path around 45° to the vertical direction. In Fig. 13(a) and (b), it is noted that the shear planes form at the concrete dowels. The upper shear plane has larger plastic strains, indicating that the concrete dowels can help to decrease the separation between steel beams and concrete blocks.

3.4. Parameter study

For further exploring the lateral shear behavior and proposing

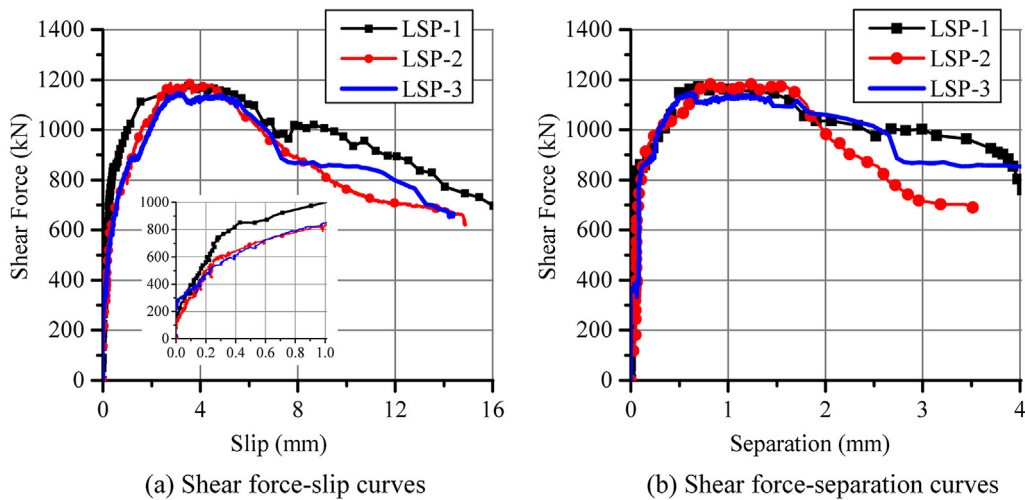


Fig. 6. Shear force-deformation curves.

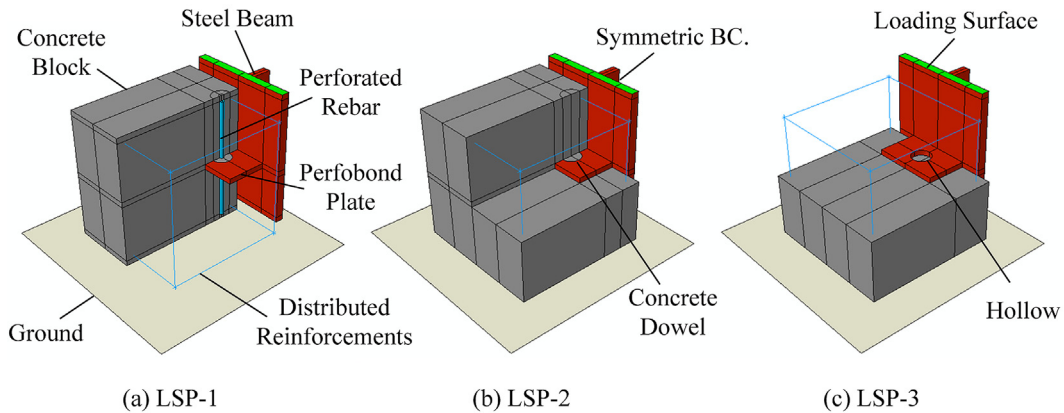


Fig. 7. Finite element models.

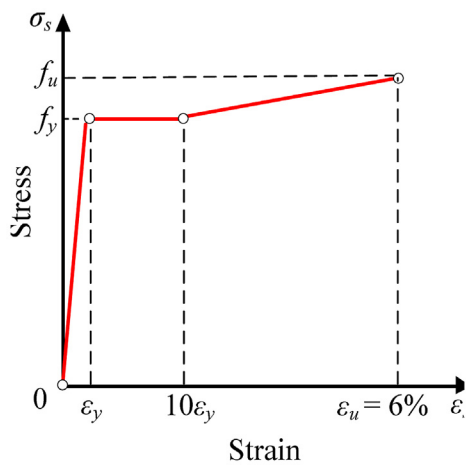


Fig. 8. Stress-strain curve of steel.

analytical models, parameter study with a total of 144 models was performed based on the validated modeling method. In the parametric study, the cohesive behavior was eliminated. Additional variables were considered in the extended calculations, including the height, length, and thickness of perfbond plates, and the concrete grade, as shown in Table 5. The concrete grade was

following the definition provided in CEB-FIP MC2010. Only the practicable parameters in applications were chosen to make the results representative. The diameters of holes, as well as the diameters of perforated rebars varied with the plate height. For the perfbond plates with the heights of 50 and 100 mm, the diameters of holes were chosen as 25 and 50 mm, respectively. The 150 and 200 mm high perfbond plates employed the holes with a diameter of 75 mm. In this investigation, the holes were always located at the center of the plates. With regards to the perforated rebars, the diameter of perforated rebars was taken as 20 mm except for the cases with a hole diameter of 25 mm. On the concern of practical applications, the diameter of perforated rebar for those cases equaled 10 mm [14].

Fig. 14 shows the representative results of the parametric study, involving the effects of all the parameters on the lateral shear capacity and stiffness. Fig. 14(a) shows the shear force-slip curves of the models with varying plate heights, where the plate length and thickness are 200 mm and 20 mm, and the concrete grade is C40. The solid black line represents the load that leads to the yielding of the perfbond plates. The results showed that the model with a height of 50 mm has a significantly smaller peak slip and worse ductility than the other three models. The reason is that the shear capacity of the 50 mm-height model is lower than the load that leads to the yielding of plates so that the brittle concrete crushing occurs. On the contrary, the other three models present larger peak slips and better ductility. It is noted that the 200 mm-height model

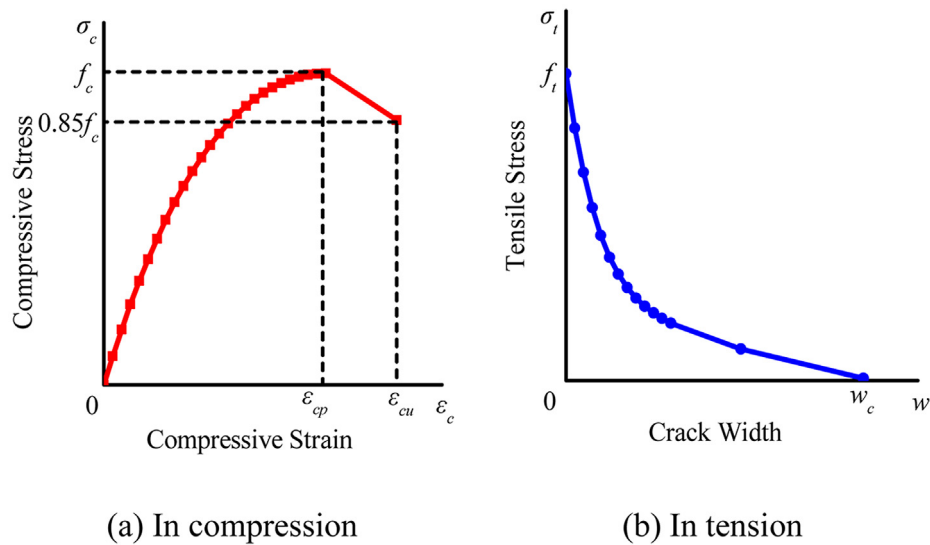


Fig. 9. Constitutive laws of concrete.

has a larger remained strength under the large slips. The reason is the hole in this model is more away from the fillet welds, which improves the uplift behavior and enlarges the ductility of the lateral shear behavior of PBLs. Fig. 14(b) and (c) presents the effects of plate height and length on the lateral shear strength and stiffness. The plate length significantly influences the shear strength and stiffness, while the plate height only has a slight impact on the shear strength and is almost irrelevant to the stiffness.

Fig. 14(d) shows the shear force-slip curves of the models with varying concrete compressive strength, where the plate height, length, and thickness are 200 mm, 150 mm, and 20 mm, respectively. The solid red line represents the load that leads to the fracture of the perfobond plates. The models with the concrete strength higher than 58 MPa have the same shear capacity, which equals the load that leads to the fracture of the perfobond plates. The reason is that the failure modes in these models are the fractures of plates instead of concrete crushing. The embedded figures also demonstrate that under the load of shear capacity, most parts of the plate cross-section have the Mises stress close to the ultimate strength of steel. Therefore, the lateral shear capacity of PBLs is limited by the shear fracture strength of plates. Fig. 14(e) and (f) depict the effects of concrete grades and plate thickness on the lateral shear strength and stiffness. The solid lines in Fig. 14(e) are the shear fracture strength of plates. The results show that the concrete strength and the plate thickness affect the shear strength and stiffness, but the upper limit of shear strength exists.

4. Theoretical analyses

4.1. Lateral shear capacity

Based on the parametric study above, the lateral shear capacity of PBLs is mainly contributed by the bearing actions between perfobond plates and concrete blocks, especially at the region close to fillet welds. The longitudinal length and thickness of perfobond plates and the compressive strength of concrete are the major influential factors on the shear capacity, while the height of plates has a minor impact. Since the plate area is not the dominant fact, and the circle holes of PBLs are usually located at the center of plates, the impact of holes with practicable diameters on the lateral shear capacity is negligible. Also, for the cases that the plate fractures instead of the concrete crushing, the shear capacity is limited

by the shear fracture failure of perfobond plates.

Since the failure mode of PBLs under lateral shear loading is similar to those of channel and angle shear connectors [30–33] as shown in Fig. 15, the development of shear capacity equations for channel and angle connectors is introduced and referred.

According to the push-out test results, Slutter and Driscoll [34] proposed the shear capacity equation (4) for channel shear connectors, which is included in American AISC 360-05 [35]. The expression considers the nonlinear effects of both concrete strength and elastic modulus, while the thickness and length of channels have a linear relationship with the shear capacity.

$$V_n = \eta (t_f + 0.5t_w) L_c \sqrt{f_c E_c} \quad (4)$$

where V_n is the shear capacity; t_f and t_w are the thickness of channel flanges and webs, respectively; L_c is the longitudinal length of shear connectors; f_c and E_c are the concrete compressive strength and modulus; η is the coefficient that equals 0.3.

Canadian code CAN/CSA-S16-01 [36] contains Eq. (5) which has a similar form to Eq. (4) for the shear capacity of channel connectors. The difference is that Eq. (5) only takes the effect of the concrete compressive strength into account, while ignores the effect of elastic modulus.

$$V_n = 36.5 (t_f + 0.5t_w) L_c \sqrt{f_c} \quad (5)$$

Based on 58 groups of push-out tests, Yokota et al. [37] studied the shear behavior of angle connectors and presented the shear capacity equation (6). Yamada et al. [38] also conducted push-out tests on angle connectors and put forward Eq. (7) with the same form as Eq. (6). In Eqs. (6) and (7), the shear capacity is linear with the length of angle connectors and the square roots of angle thickness and concrete strength.

$$V_n = 88L_c \sqrt{t_w f_c} \quad (6)$$

$$V_n = 65L_c \sqrt{t_w f_c} \quad (7)$$

Khalilian et al. [39] carried out push-out tests and FEA parametric analyses on angle connectors. Based on the test and numerical results, they put forward the shear capacity equation (8) where the shear resistance is nonlinearly influenced by the length

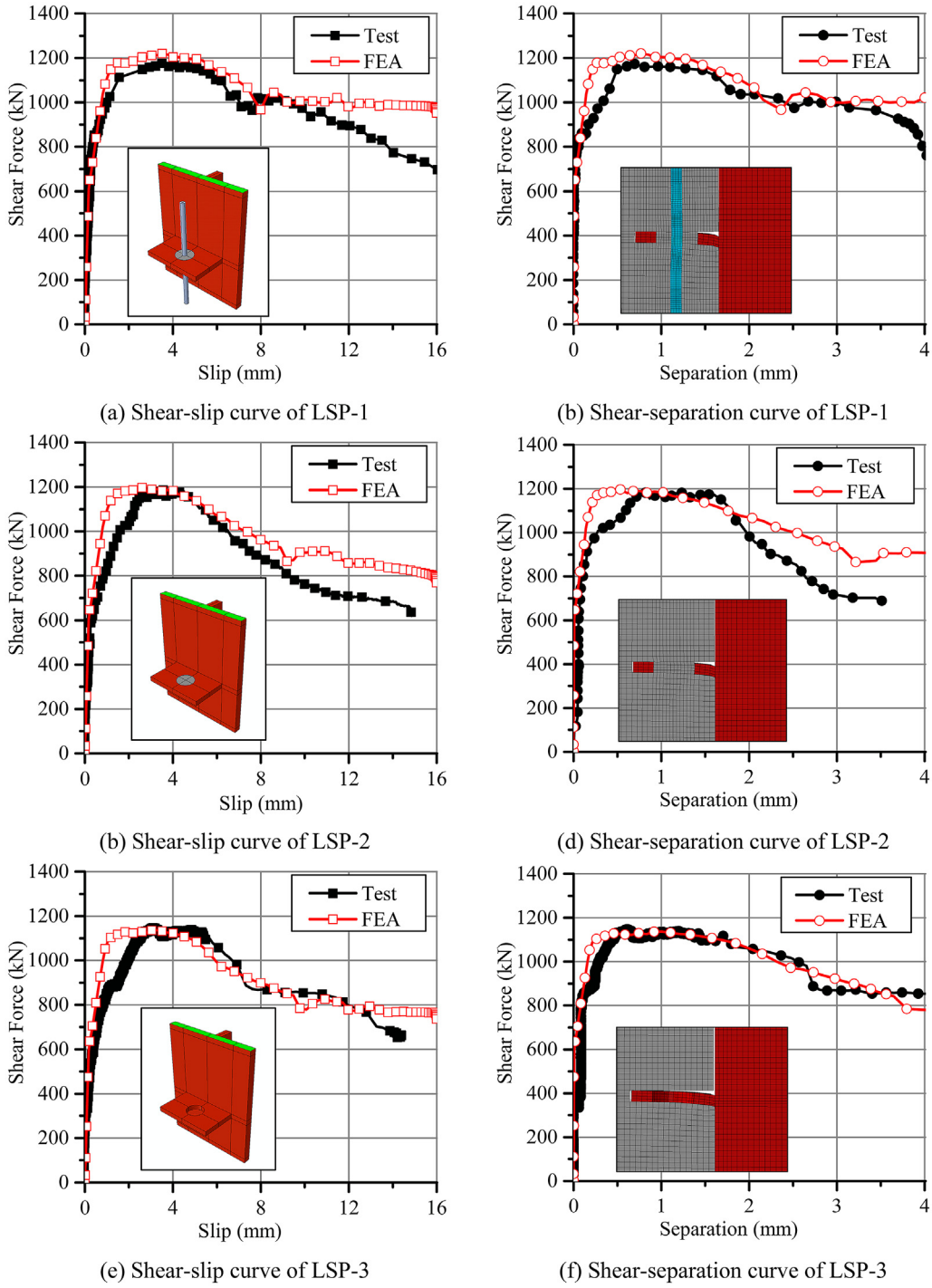


Fig. 10. Model validations.

and thickness of angles and the concrete strength. Meanwhile, the shear capacity is limited to be smaller than the shear strength of webs related to the connector tensile strength f_u .

$$V_n = 4300L_c^{0.64}t_w^{0.27}f_c^{0.11} \leq 0.6f_u t_w L_c \quad (8)$$

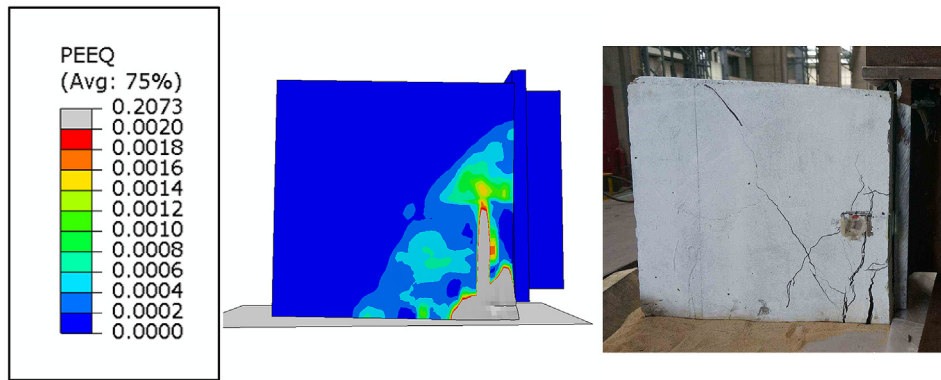
Referred to the parametric FEA results and the equations above, the authors propose the lateral shear capacity expression (9) for PBLs, where V_l is the lateral shear capacity; l , h , and t are the length, height, and thickness of perfobond plates, respectively. The coefficients in the equation are obtained based on the numerical results of 144 FEA models after validation of experimental results. Compared with Eqs. (4) and (5) for channel connectors, the proposed equation considers that the thickness of perfobond plates non-linearly affects the shear capacity. Besides, although the effect is

slight when the plate has adequate height, the contribution of the plate height is taken into account in the put forward expression compared with Eqs. (6) and (7) for angle connectors. The upper bound of the shear capacity corresponding to the plate fracture failure mode is also provided in Eq. (9). Fig. 16 compares the calculated results by Eq. (9) with the numerical results, where the coefficient of determination is 0.96. The mean ratio of calculated results to numerical results is 0.99, and the standard deviation is 0.06.

$$V_l = 0.1lh^{0.1}\sqrt{f_c t} \leq 0.6f_u t l \quad (9)$$



(a) Yielding of perfbond plates



(b) Cracking on concrete blocks

Fig. 11. Comparison of failure modes.

4.2. Lateral shear stiffness

As for the deformation behavior, perfbond plates with a unit length can abstract to a beam supported by the elastic foundation. Fig. 17 shows the mechanical model for the perfbond plate with a unit length, where the surrounding concrete is regarded as a continuous elastic medium. In the figure, $y(x)$ is the deflection of any location that is x away from the fillet welds; k is the supportive stiffness of a unit length. The impacts of circle holes and perforated rebars are temporarily ignored and will be taken into account later by using a coefficient.

To simplify the derivation of the lateral shear stiffness of PBLs, the following assumptions are made:

- (1) The bending of perfbond plates conforms to the plane cross-section assumption;
- (2) The foundation reaction force is linear with the vertical deflection (Winkler's hypothesis);
- (3) Steel and concrete are at elastic states;
- (4) Ignoring the frictional forces at the interfaces between steel plates and concrete.

The mechanical model of an element with a length of d_x is also shown in Fig. 17. The left and right sides of the element are respectively applied the shear forces $Q, Q+dQ$, and the moments $M, M+dM$. The foundation reaction force p acts on the bottom of the element. Based on the force and moment equilibrium conditions, the following equations are addressed:

$$p = \frac{dQ}{dx}; Q = \frac{dM}{dx} \tag{10}$$

$$p = \frac{d^2M}{dx^2} \tag{11}$$

$$p = ky \tag{12}$$

By the elastic assumption of steel plates, the cross-sectional moment is linear with the flexural stiffness $E_s I_s$. Substituting Eqs. (12) and (13) into Eq. (11), the differential equation of the elastic foundation beam deflection is obtained:

$$M = -E_s I_s \frac{d^2y}{dx^2} \tag{13}$$

$$\frac{d^4y}{dx^4} + \frac{k}{E_s I_s} y = 0 \tag{14}$$

Assume the characteristic parameter $\beta = \sqrt[4]{k/(4E_s I_s)}$. The supportive stiffness is assumed to be relevant to the concrete modulus [23], e.g., $k = cE_c$, where c is an undetermined coefficient. Thus, the general solution of Eq. (14) is:

$$y = e^{\beta x}(C_1 \sin \beta x + C_2 \cos \beta x) + e^{-\beta x}(C_3 \sin \beta x + C_4 \cos \beta x) \tag{15}$$

The considered boundary conditions are: (1) the rotation angle at $x = 0$ is 0; (2) the applied shear force at $x = 0$ is V ; (3) the

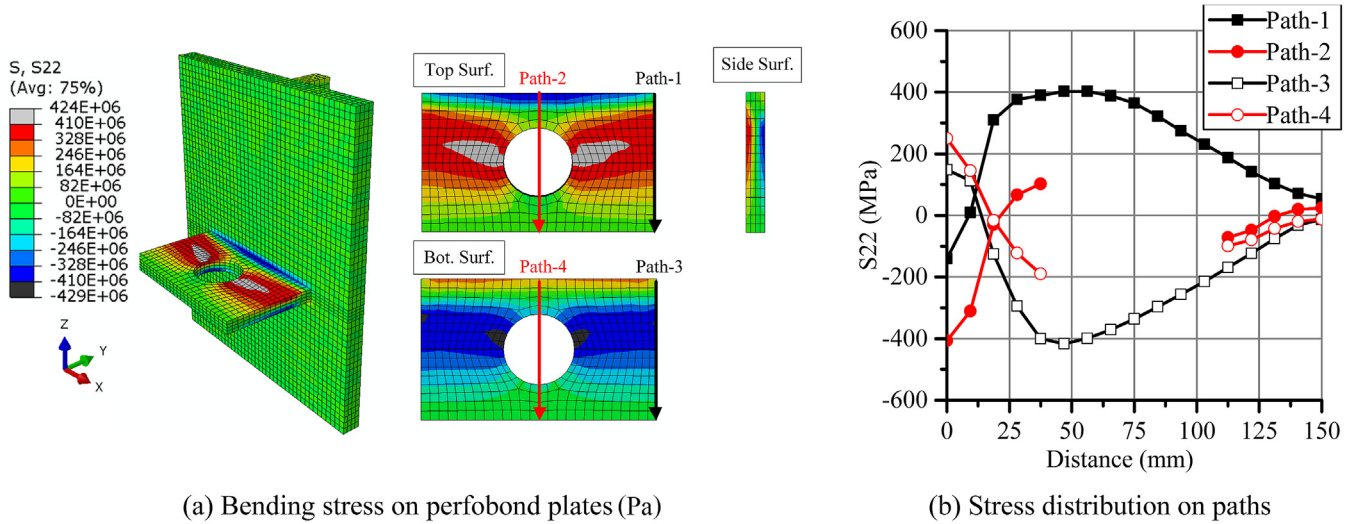


Fig. 12. Shear mechanism of perforated plates.

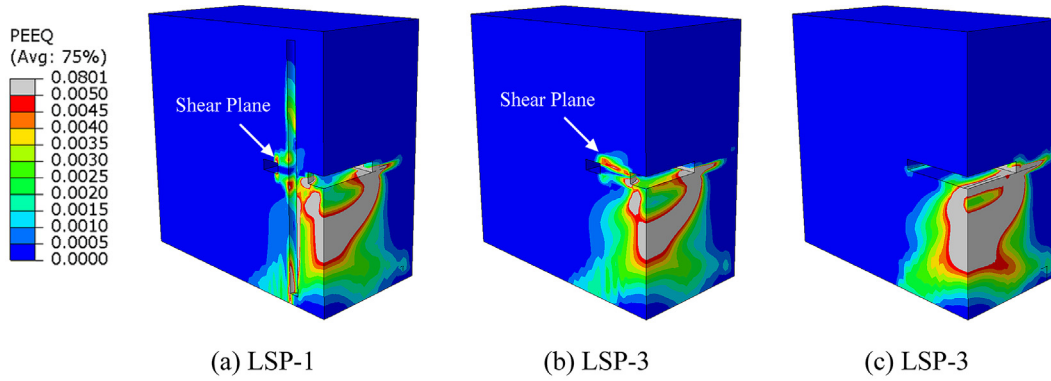


Fig. 13. Plastic strains in concrete blocks.

Table 5
Variables in parametric study.

Plate Height <i>h</i> (mm)	50, 100, 150, 200
Hole Diameter <i>d</i> (mm)	25, 50, 75
Perforated Rebar Diameter <i>d_s</i> (mm)	10, 20
Plate Length <i>l</i> (mm)	150, 200, 250
Plate Thickness <i>t</i> (mm)	16, 20, 25
Concrete Grade	C30, C40, C50, C60

$$V_h = 0: C_1 e^{\beta h} (\cos \beta h - \sin \beta h) - C_2 e^{\beta h} (\cos \beta h + \sin \beta h) + C_3 e^{-\beta h} (\cos \beta h + \sin \beta h) + C_4 e^{-\beta h} (\cos \beta h - \sin \beta h) = 0 \quad (19)$$

To simplify the derivation, assume the parameter B_1 to B_4 as follows and substitute the parameters into Eqs. (18) and (19).

$$\begin{cases} B_1 = e^{\beta h} \sin \beta h \\ B_2 = e^{\beta h} \cos \beta h \\ B_3 = e^{-\beta h} \sin \beta h \\ B_4 = e^{-\beta h} \cos \beta h \end{cases} \quad (20)$$

$$y''_h = 0: B_2 C_1 - B_1 C_2 - B_4 C_3 + B_3 C_4 = 0 \quad (21)$$

$$V_h = 0: (B_2 - B_1)C_1 - (B_1 + B_2)C_2 + (B_3 + B_4)C_3 - (B_3 - B_4)C_4 = 0 \quad (22)$$

Rewrite the boundary conditions as a matrix and solve the parameter C_1, C_2, C_3, C_4 , so that the vertical displacement at the left end is obtained:

curvature at $x = h$ is 0; (4) the shear force at $x = h$ is 0.

$$y'_0 = 0: C_1 + C_2 + C_3 - C_4 = 0 \quad (16)$$

$$V_0 = V: C_1 - C_2 + C_3 + C_4 = \frac{V}{2\beta^3 E_s I_s} \quad (17)$$

$$y''_h = 0: e^{\beta h} (C_1 \cos \beta h - C_2 \sin \beta h) - e^{-\beta h} (C_3 \cos \beta h - C_4 \sin \beta h) = 0 \quad (18)$$

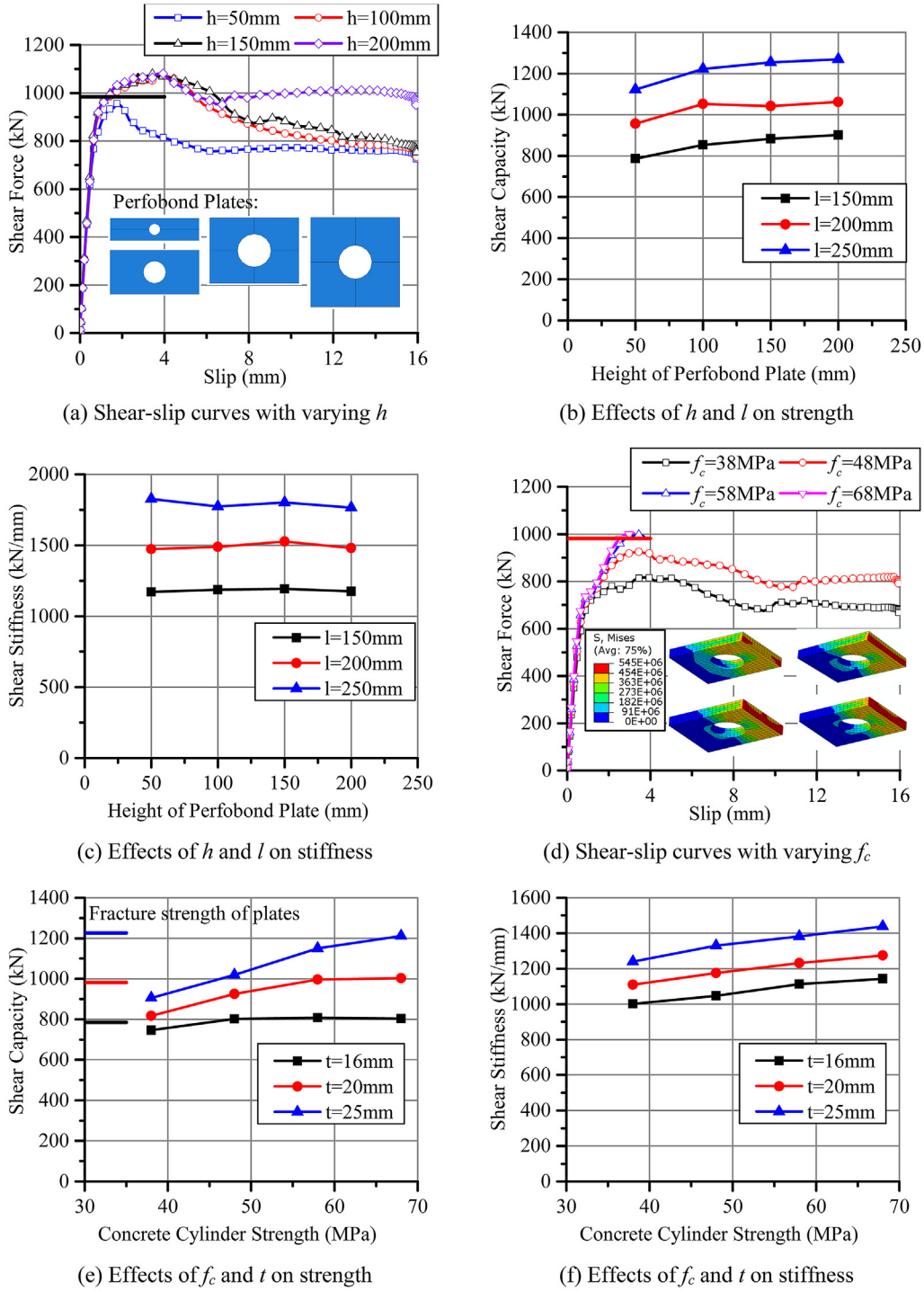


Fig. 14. Results of parametric study.

$$\begin{bmatrix} B_2 & -B_1 & -B_4 & B_3 \\ (B_2 - B_1) & -(B_1 + B_2) & (B_3 + B_4) & -(B_3 - B_4) \\ 1 & 1 & 1 & -1 \\ 1 & -1 & 1 & 1 \end{bmatrix} \begin{bmatrix} C_1 \\ C_2 \\ C_3 \\ C_4 \end{bmatrix} = \begin{bmatrix} 0 \\ 0 \\ 0 \\ \frac{V}{2\beta^3 E_s I_s} \end{bmatrix} \quad (23)$$

$$y_0 = C_2 + C_4 = \frac{V}{4\beta^3 E_s I_s} \frac{2B_1 B_3 + 6B_2 B_4 + B_1^2 + B_2^2 + B_3^2 + B_4^2}{2B_1 B_4 + 2B_2 B_3 + B_1^2 + B_2^2 - B_3^2 - B_4^2}$$

$$y_0 = \frac{V}{4\beta^3 E_s I_s} \frac{4 + 2 \cos 2 \beta h + e^{2\beta h} + e^{-2\beta h}}{e^{2\beta h} + e^{-2\beta h} + 2 \sin 2 \beta h} \quad (24)$$

According to the definition of shear stiffness, the lateral shear stiffness equation of PBLs with a unit length is as Eq. (25). Further, the stiffness equation for the entire PBLs can be presented as Eq. (26), where α is an undetermined coefficient considering the effects of plate length, concrete dowels, perforated rebars, etc.

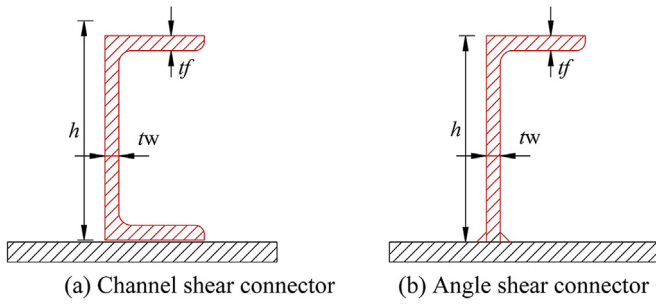


Fig. 15. Channel and angle shear connectors.

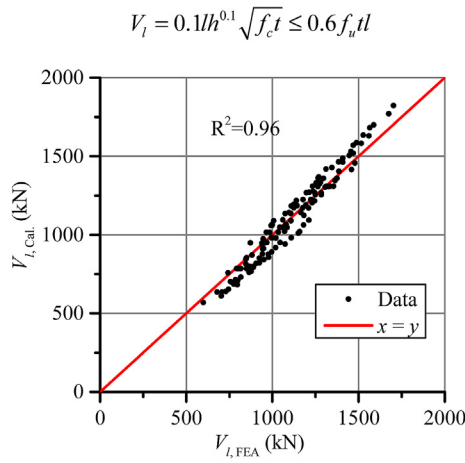


Fig. 16. Comparison between FEA and Eq. (9).

$$\bar{k}_l = \frac{V}{y_0} = 4\beta^3 E_s I_s \frac{2 \sin 2\beta h + e^{2\beta h} + e^{-2\beta h}}{4 + 2 \cos 2\beta h + e^{2\beta h} + e^{-2\beta h}} \quad (25)$$

$$k_l = \bar{k}_l l = \alpha \beta^3 E_s I_s l \frac{2 \sin 2\beta h + e^{2\beta h} + e^{-2\beta h}}{4 + 2 \cos 2\beta h + e^{2\beta h} + e^{-2\beta h}} \quad (26)$$

By fitting the numerical results of 144 models, the coefficient c in the characteristic parameter β equals 0.2, and the coefficient α is 0.25 (Fig. 18). The fraction part of Eq. (26) is defined as the parameter γ . By substituting β into γ , the value of γ under the practicable component sizes and material properties is close to constant 1. That means the height of plates has negligible effects on the lateral shear stiffness. Based on the nature of γ , the equation can

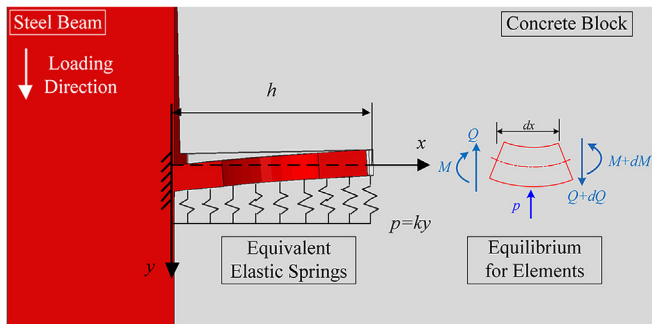


Fig. 17. Elastic foundation beam mechanical model.

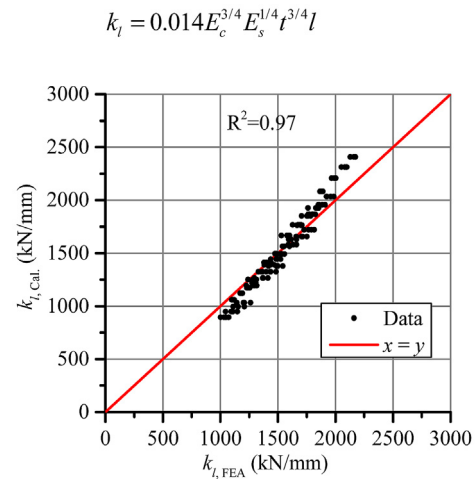


Fig. 18. Comparison between FEA and Eq. (29).

be simplified as Eq. (28).

$$\gamma = \frac{2 \sin 2\beta h + e^{2\beta h} + e^{-2\beta h}}{4 + 2 \cos 2\beta h + e^{2\beta h} + e^{-2\beta h}} \approx 1 \quad (27)$$

$$k_l = 0.25\beta^3 E_s I_s l \quad (28)$$

Finally, by substituting $\beta = \sqrt[4]{0.2E_c/(4E_s I_s)}$ and $I_s = t^3/12$, the simplified lateral shear stiffness equation (29) is proposed. Fig. 18 compares the calculated results by Eq. (29) with the numerical results, where the coefficient of determination is 0.97. The mean ratio of calculated results to numerical results is 0.99, and the standard deviation is 0.07.

$$k_l = 0.014 E_c^{3/4} E_s^{1/4} t^{3/4} l \quad (29)$$

5. Conclusion

This paper documents three push-out tests on the out-of-plane shear behavior of PBLs. The effects of perforated rebars and concrete dowels on the lateral shear capacity, stiffness, and ductility were discussed. Then, parametric FE models for the push-out tests were built and validated based on the test results. The influences of the height, length, and thickness of perfbond plates and the concrete compressive strength on the lateral shear behavior were evaluated. Finally, based on the existing shear capacity equations for channel and angle connectors, and the theory of elastic foundation beams, the expressions for the lateral shear capacity and stiffness of PBLs were put forward. The following conclusions could be drawn:

- (1) The failure mode of the specimens was the crushing of concrete under the perfbond plates. At the failure, the perfbond plates had yielded but not fractured. Since the plastic deformation of perfbond plates developed, the peak slips of specimens were larger than 3 mm. PBLs presented good ductility under lateral shear forces.
- (2) Perforated rebars and concrete dowels hardly affect the lateral shear capacity of PBLs. The reason is that the holes are usually located at the center of plates and most of the applied loads are undertaken by the region around the perfbond plate-flange fillet weld. However, perforated rebars and concrete dowels improve the lateral ductility of PBLs as well

as decrease the separations between steel beams and concrete blocks. Compared with LSP-1, the lateral shear stiffness of LSP-2 (without perforated rebars) and LSP-3 (without concrete dowels) reduce 7.7% and 13.6%.

- (3) Based on the parametric study, the models with the failure mode that concrete crushing occurs before the yielding of perfobond plates show the smaller peak slips and worse ductility. The lateral shear capacities of PBLs are limited to the shear fracture strength of plates. The plate length significantly affects the shear strength and stiffness, while the plate height only has a slight impact on the shear strength and is irrelevant to the stiffness. Both the concrete strength and the plate thickness affect the shear strength and stiffness.
- (4) In the proposed equations, the lateral shear capacity is mainly related to the plate length and thickness, and concrete compressive strength. The significant factors on the lateral shear stiffness are the length, thickness, and modulus of perfobond plates, and concrete modules.

6. Future works

As the shear connectors usually undertake considerable longitudinal shear forces, the combined longitudinal-transverse response and even the combined longitudinal-transverse-uplift performance of PBLs should be revealed and discussed. Additional experimental studies for predicting the structural behavior of PBLs under combined loads will be presented in future works.

Appendix A. Supplementary data

Supplementary data to this article can be found online at <https://doi.org/10.1016/j.jcsr.2019.105850>.

References

- [1] Y. Liu, H. Xin, J. He, D. Xue, B. Ma, Experimental and analytical study on fatigue behavior of composite truss joints, *J. Constr. Steel Res.* 83 (2013) 21–36.
- [2] Y. Liu, H. Xin, Y. Liu, Load transfer mechanism and fatigue performance evaluation of suspender-girder composite anchorage joints at serviceability stage, *J. Constr. Steel Res.* 145 (2018) 82–96.
- [3] S.H. Kim, C.G. Lee, J.H. Ahn, J.H. Won, Experimental study on joint of spliced steel–PSC hybrid girder, Part I: proposed parallel-perfobond-rib-type joint, *Eng. Struct.* 33 (8) (2011) 2382–2397.
- [4] J. He, Y. Liu, B. Pei, Experimental study of the steel-concrete connection in hybrid cable-stayed bridges, *J. Perform. Constr. Facil.* 28 (3) (2013) 559–570.
- [5] S. He, Z. Fang, Y. Fang, M. Liu, L. Liu, A.S. Mosallam, Experimental study on perfobond strip connector in steel–concrete joints of hybrid bridges, *J. Constr. Steel Res.* 118 (2016) 169–179.
- [6] Y. Li, Y. Liu, F. Wang, F. Yang, Load transfer mechanism of hybrid pylon joint with cells and bearing plates, *Adv. Civ. Eng.* 2018 (2018).
- [7] S.H. Kim, C.G. Lee, J.H. Ahn, J.H. Won, Experimental study on joint of spliced steel–PSC hybrid girder, Part I: proposed parallel-perfobond-rib-type joint, *Eng. Struct.* 33 (8) (2011) 2382–2397.
- [8] J. He, Y. Liu, A. Chen, T. Yoda, Mechanical behavior and analysis of composite bridges with corrugated steel webs: state-of-the-art, *International Journal of Steel Structures* 12 (3) (2012) 321–338.
- [9] T. Hosaka, K. Mitsuki, H. Hiragi, Y. Ushijima, Y. Tachibana, H. Watanabe, An experimental study on shear characteristics of perfobond strip and its rational strength equations, *J. Struct. Eng. JSCE* 46 (2000) 1593–1604.
- [10] S.B. Medberry, Perfobond shear connector for composite construction, *Eng. J.* 39 (2002).
- [11] S.Y.K. Al-Darzi, A.R. Chen, Y.Q. Liu, Finite element simulation and parametric studies of perfobond rib connector, *Am. J. Appl. Sci.* 4 (3) (2007) 122–127.
- [12] J.H. Ahn, C.G. Lee, J.H. Won, S.H. Kim, Shear resistance of the perfobond-rib shear connector depending on concrete strength and rib arrangement, *J. Constr. Steel Res.* 66 (10) (2010) 1295–1307.
- [13] J.P.S. Cândido-Martins, L.F. Costa-Neves, P.D.S. Vellasco, Experimental evaluation of the structural response of Perfobond shear connectors, *Eng. Struct.* 32 (8) (2010) 1976–1985.
- [14] S. Zheng, Y. Liu, T. Yoda, W. Lin, Parametric study on shear capacity of circular-hole and long-hole perfobond shear connector, *J. Constr. Steel Res.* 117 (2016) 64–80.
- [15] H. Allahyari, I.M. Nikbin, R.R. Saman, et al., A new approach to determine strength of Perfobond rib shear connector in steel-concrete composite structures by employing neural network, *Eng. Struct.* 157 (2018) 235–249.
- [16] J.P.C. Rodrigues, L. Laím, Behaviour of perfobond shear connectors at high temperatures, *Eng. Struct.* 33 (10) (2011) 2744–2753.
- [17] I.B. Valente, P.J. Cruz, Experimental analysis of shear connection between steel and lightweight concrete, *J. Constr. Steel Res.* 65 (10–11) (2009) 1954–1963.
- [18] S. He, Z. Fang, A.S. Mosallam, Push-out tests for perfobond strip connectors with UHPC grout in the joints of steel-concrete hybrid bridge girders, *Eng. Struct.* 135 (2017) 177–190.
- [19] Z. Xiong, Y. Liu, Y. Zuo, H. Xin, Shear performance assessment of sand-coated GFRP perforated connectors embedded in concrete, *Materials* 12 (12) (2019) 1906.
- [20] S.H. Kim, K.T. Choi, S.J. Park, S.M. Park, C.Y. Jung, Experimental shear resistance evaluation of Y-type perfobond rib shear connector, *J. Constr. Steel Res.* 82 (2013) 1–18.
- [21] X. Wang, Y. Liu, Y. Liu, Experimental study on shear behavior of notched long-hole perfobond connectors, *Adv. Struct. Eng.* 22 (1) (2019) 202–213.
- [22] Y. Liu, H. Xin, Y. Liu, Experimental and analytical study on shear mechanism of rubber-ring perfobond connector, *Eng. Struct.* 197 (2019) 109382.
- [23] S.J. Zheng, Y.Q. Liu, Experiment of initial shear stiffness of perfobond connector, *China J. Highw. Transp.* 27 (11) (2014) 69–75.
- [24] EUROCODE 4, EN 1994-1-1, Design of Composite Steel and Concrete Structures Part 1.1 General Rules and Rules for Buildings, CEN-European Committee for Standardization, Brussels, 2005.
- [25] C. Standard, Code for Design of Concrete Structures (GB 50010-2010), China Building Industry Press, Beijing, China, 2010.
- [26] ABAQUS Documentation, Version 6.12, Dassault system, USA, 2012.
- [27] CEB-FIP Model Code 2010, British Standard Institution, 2010.
- [28] H.T. Nguyen, S.E. Kim, Finite element modeling of push-out tests for large stud shear connectors, *J. Constr. Steel Res.* 65 (10–11) (2009) 1909–1920.
- [29] D.A. Hordijk, Tensile and tensile fatigue behaviour of concrete; experiments, modelling and analyses, *Heron* 37 (1992).
- [30] S. Maleki, M. Mahoutian, Experimental and analytical study on channel shear connectors in fiber-reinforced concrete, *J. Constr. Steel Res.* 65 (8–9) (2009) 1787–1793.
- [31] M. Shariati, N.R. Sulong, M. Suhatri, A. Shariati, M.A. Khanouki, H. Sinaei, Comparison of behaviour between channel and angle shear connectors under monotonic and fully reversed cyclic loading, *Constr. Build. Mater.* 38 (2013) 582–593.
- [32] M. Shariati, N.R. Sulong, A. Shariati, A.B.H. Kueh, Comparative performance of channel and angle shear connectors in high strength concrete composites: an experimental study, *Constr. Build. Mater.* 120 (2016) 382–392.
- [33] M. Paknahad, M. Bazzaz, M. Khorami, Shear capacity equation for channel shear connectors in steel-concrete composite beams, *Steel Compos. Struct., Int. J.* 28 (4) (2018) 483–494.
- [34] R.G. Slutter, G.C. Driscoll, Flexural strength of steel-concrete composite beams, *J. Struct. Div.* 91 (2) (1965) 71–99.
- [35] ANSI/AISC 360-05, Specification for Structural Steel Buildings, American Institute of Steel Construction, 2005.
- [36] CANCSA-S16-01, Limit States Design of Steel Structures, Canadian Standards Association (CSA), 2001.
- [37] H. Yokota, Load carrying capacity of shear connectors made of shape steel in steel-concrete composite members. Technical Note of the Port and Harbor Research Institute, Ministry of Transport (595) (1989) 3–24.
- [38] M. Yamada, O. Kiyomiya, Experimental study on the loading capacity of L-shape and headed stud shear connector for composite structures, *Trans Jpn Concr Inst JCI* 14 (1992) 461–468.
- [39] M. Khalilian, Sharif University of Technology, The Assessment of Shear Capacity of Angle Shear Connectors, 2013.